Scaling High-Order Harmonic Generation from Laser-Solid Interactions to Ultrahigh Intensity

F. Dollar, P. Cummings, V. Chvykov, L. Willingale, M. Vargas, V. Yanovsky, C. Zulick, A. Maksimchuk, A. G. R. Thomas, and K. Krushelnick

Phys. Rev. Lett. **110**, 175002 — Published 24 April 2013

DOI: 10.1103/PhysRevLett.110.175002

Scaling high-order harmonic generation from laser-solid interactions to ultra-high intensity

F. Dollar,* P. Cummings, V. Chvykov, L. Willingale, M. Vargas, V. Yanovsky,
C. Zulick, A. Maksimchuk, A. G. R. Thomas, and K. Krushelnick
Center for Ultrafast Optical Science, University of Michigan, Ann Arbor, MI 48109-2099 USA
(Dated: April 4, 2013)

Coherent x-ray beams with sub-femtosecond ($< 10^{-15}$ seconds) pulse durations will enable measurements of fundamental atomic processes in a completely new regime. High-order harmonic generation (HOHG) using short pulse (< 100 fs) infrared lasers focused to intensities surpassing 10^{18} Wcm^{-2} onto a solid density plasma is a promising means of generating such short pulses. Critical to the relativistic oscillating mirror mechanism is the steepness of the plasma density gradient at the reflection point, characterized by a scale length, which can strongly influence the harmonic generation mechanism. It is shown that for intensities in excess of 10^{21} Wcm^{-2} that an optimum density ramp scale length exists that balances an increase in efficiency with a growth of parametric plasma wave instabilities. We show that for these higher intensities, the optimal scale length is c/ω_0, for which a variety of HOHG properties are optimized, including: total conversion efficiency; HOHG divergence; and their power law scaling. Particle-in-cell simulations show striking evidence of the HOHG loss mechanism through parametric instabilities and relativistic self-phase-modulation, which affect the produced spectra and conversion efficiency.

PACS numbers: 52.59.Ye, 52.38.Dx, 52.38.Ph, 52.65.Rr

High intensity laser-plasma interactions have recently shown that high brightness x-ray production in the soft and hard x-ray regimes are achievable through a variety of mechanisms, such as betatron generation from laser wakefield acceleration [1] and high-order harmonic generation (HOHG) from under-dense gas plasmas [2]. Harmonic generation occurs for solid density interactions when the surface electrons are oscillated by an intense laser field to relativistic speeds, and the resulting nonlinearity gives rise to the re-radiation of harmonics of the fundamental laser frequency [3–9]. The first solid density experiments were performed with CO_2 lasers over 25 years ago [10, 11]. HOHG up to several hundred times of the fundamental laser frequency [12] was demonstrated using a kilojoule energy, picosecond duration laser. Short-pulse lasers ($\tau < 100$ fs) interactions with solid density targets have unique advantages for HOHG, being more compact and possessing higher repetition rates with significant laser power [13]. Recently, dense bunches of electrons generated at the plasma-vacuum interface have also been observed to generate harmonics through thin targets via coherent synchrotron emission [14].

While much analytical work has been performed in one dimension [5, 15, 16], our understanding under realistic conditions is limited. In particular, laser energy arriving prior to the main pulse causes heating and expansion of the target. A reasonable density function is a self-similar solution for plasma expansion into vacuum [17], given by an exponential ramp $n_e(x) = n_{e0}\exp(x/L_s)$, with the "pre-plasma" scale length, L_s. Previous experiments have shown that laser absorption and hot electron production are strongly affected by the density scale length, and can have a severely deleterious effect in HOHG experiments if not well controlled [12, 18–20]. However, it has also been observed that the HOHG efficiency can be increased by increasing the plasma scale length [21], and if the density profile is close to a step function, HOHG is suppressed [22]. 1 dimensional Particle-in-Cell simulations performed for moderate intensities ($10^{17} - -10^{20}$ Wcm^{-2}) demonstrated a resonant condition for harmonic generation with linear plasma density profiles at $L_s = 0.2\lambda$ [23].

These observations suggest that an optimal scale length exists. In this Letter, we demonstrate that in the strongly relativistic regime (i.e., normalized vector potential $a_0 = eA/mc \gg 1$) there exists an optimal scale length for HOHG. We find that as the density scale length exceeds the electron inertial length c/ω_p, the HOHG process becomes parametrically unstable, causing a loss of coherence to the harmonic structure in the x-rays. Conversely for short scale lengths, the effective spring constant of the oscillating surface is too high, which limits the Doppler shift of the reflected wave. Particle-in-cell (PIC) simulations are performed that support the experimental observations and show that absolute harmonic efficiency and divergence are also optimized at this scale length.

The experiments were performed using the HERCULES laser facility at University of Michigan, a Ti:Sapphire system ($\lambda = 800$ nm) producing pulses with $\tau = 40$ fs duration full-width at half-maximum (FWHM) with an amplified spontaneous emission (ASE) intensity contrast of 10^{-11} [24]. 1.5 J (± 0.2) were delivered to the target with $\sim 60\%$ of the energy in a 1.2 μm FWHM focal spot via an $f/1$ off-axis parabolic mirror (OAP) and a deformable mirror correcting the wavefront to result in a measured Strehl ratio of between 0.6 and 0.99.

The on-target intensity was $2\times10^{21}\mathrm{Wcm}^{-2}$ (corresponding to $a_0 = 30$). Prior to the experimental chamber, mirrors focused the amplified pulse onto a pair of anti-reflection coated BK7 glass substrates acting as plasma mirrors [25, 26]. Each plasma mirror reflects $< 0.15\%$ of low intensity light while possessing a measured reflectivity of 65%–70% at high intensity, producing a ns-level ASE contrast of $< 10^{-15}$ [27]. This contrast improvement prevented preplasma formation until ~ 1 ps before the main pulse interaction, maintaining a sharp density profile. With sufficiently high contrast, a well defined reflection point exists at the relativistic critical density surface (i.e., when the plasma frequency $\omega_p = \sqrt{\frac{n_e e_c^2}{\epsilon_0 \gamma m_e}}$ equals the laser frequency ω_0).

To control L_s, one or both plasma mirrors were replaced with a higher reflectivity optic (1.5%). In situ density control was also performed by using a secondary beam with a 63 ps delay and a variable intensity between 10^{12} and 10^{16} Wcm^{-2}. Optically polished fused silica and silicon wafer were used as the targets, with the substantial difference in damage threshold providing another means of controlling density. The experimental L_s was inferred from one dimensional hydrodynamic simulations [28], which showed that L_s varied from 13 nm to 2.5 μm, corresponding to $\lambda/60$ to 3λ. In the following experimental and simulation sections, L_s is defined along the laser propagation direction rather in the target normal. However, experimental control of L_s was very difficult, since small fluctuations in the prepulse intensity around the damage threshold can cause L_s to change by hundreds of nm.

The primary HOHG detector was a flat-field EUV spectrometer, which consisted of a variable line space concave grating (Hitachi, 1,200 lines per mm) that diffracted and focused the harmonic light onto the detector, a CCD camera (Andor). The spectrometer has a resolving power of up to $1,200\ \frac{\lambda}{\Delta\lambda}$ for the wavelength range 15-25 nm, and subtended an angle of 1.7×10^{-5} sr. 800 nm of Al or 150 nm of Zr was used to filter out optical light. The detector was time-integrated, so in addition to the harmonic signal continuum and line emission was also detected from the plasma, resulting in the bright noise near the absorption edge in Fig. 1. The brightness of the Oxygen 4^+ line emission and the continuum emission scaled with L_s.

Three distinct regimes of harmonic generation were experimentally observed, whether coarse (i.e. changing plasma mirrors and target material) and fine (i.e. using a second, independent heating pulse) control of L_s was used (Fig. 1). The shortest L_s of $\lambda/60$ was obtained with no introduced prepulse and a fused silica target. For this "ultra-clean" case, very little was detected within the spectral range of the detector for 38 shots, although some shots showed evidence of weak low order harmonics (9 out of 38). Response corrected spectra are shown in Fig. 1 (a). Under these "ultra-clean" conditions, the density profile was too steep to efficiently produce harmonics.

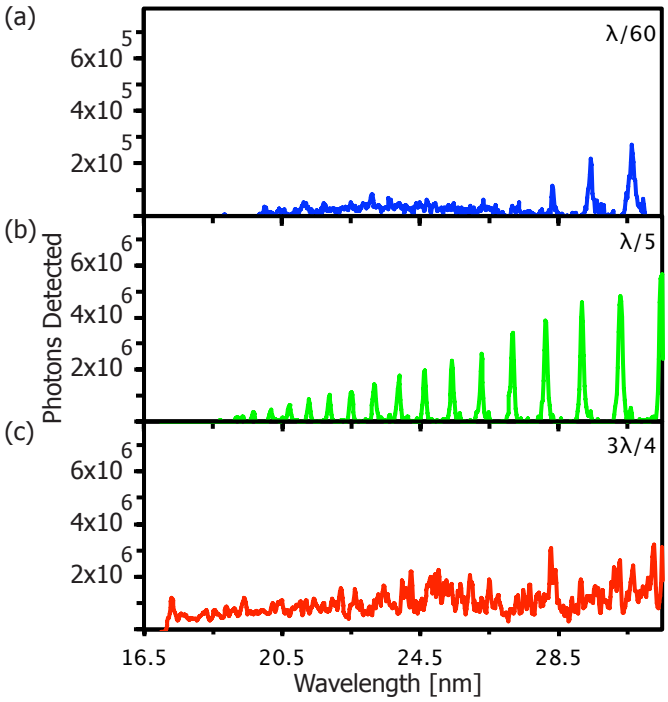

FIG. 1. (Color online) Response corrected lineouts for (a) an ultra-sharp density profile of $\lambda/60$, (b) a nominal $\lambda/5 \approx c/\omega_0$ scale length, and (c) a longer $3\lambda/4$ scale length. Note the Al filter blocks light below 17.2 nm.

Either by switching to the silicon wafer target, or by introducing the independent prepulse, an L_s of approximately $\lambda/5$ nm can be achieved. For this increased L_s, a clear and spectrally intense harmonic structure was observed, Fig. 1 (b). Harmonics up to the 60th order were clearly observed, limited by the signal-to-noise caused by the continuum radiation. Generating particularly bright harmonics such as those shown in Fig. 1 (b) was not as consistent as the other conditions, appearing in 42 out of 149 shots suggesting that the scale length range for this optimal HOHG was indeed narrow. Since the expansion of the plasma is strongly linked to the time that preplasma formation begins, small fluctuations in prepulse can have drastic effects on L_s.

However, for even longer L_s, the harmonic structure disappears. Although the spectral flux of the radiation is still strong, the coherence of the radiation is lost. This is observed for L_s between $3\lambda/4$, as shown in Fig. 1 (c), and 3λ. The spectral lines varied randomly in frequency and amplitude from shot to shot. This is consistent with a loss of periodicity, but strong phase modulation of the reflected wave.

The experimentally observed *relative* efficiency of the harmonic generation mechanism may be characterized by

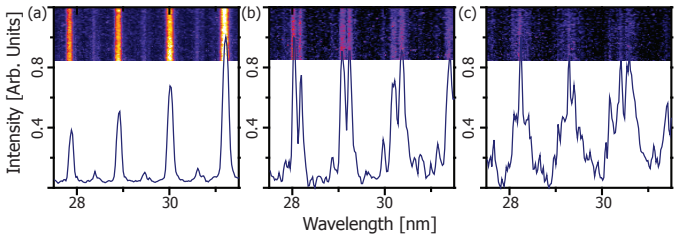

FIG. 2. (Color online) Single shot EUV spectrometer images (inlaid image) and response corrected lineouts displaying features of (a) half-harmonics, (b) sidebands, and (c) split harmonics during the transitional region of scale length. These are indicative of parametric harmonic generation from mechanisms such as SRS and TPD.

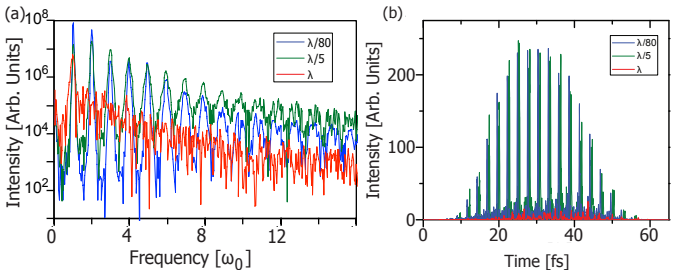

FIG. 3. (Color online) (a) Two dimensional particle-in-cell simulation power spectra for plasma scale lengths of (blue) $\lambda/80$, (green) $\lambda/5$, and (red) λ for a normalized vector potential of $a_0 = 30$ taken along the target normal. (b) 2 dimensional particle-in-cell simulations of the attosecond pulse train generated in the interaction taken along the specular direction for scale lengths of (blue) $\lambda/80$, (green) $\lambda/5$, and (red) λ.

fitting a power law scaling, n^{-p} with n the harmonic order, to the spectral intensity of the measured harmonics. To properly characterize the absolute efficiency, the angular distribution of harmonics should also be measured, however, this is expected to be a weaker function of n and would vary little over the spectral range of the detector. A fit results in $4.3 \leq p \leq 4.8$ for the optimal scale length HOHG case. For non-optimal conditions, the power law scaling ranges $5.2 \leq p \leq 10$, in agreement with previous experimental observations [22, 29, 30]. This is a faster decay than the theoretically predicted scaling of $p = \frac{8}{3}$ [36]. However, this discrepancy is likely to be a combination of the experimental conditions, including a tight focusing geometry, ion motion and a realistic plasma profile, which are not included in the analytic model.

For L_s slightly longer than optimal, features in the spectra were observed that are periodic in frequency space, as in Fig. 2. As shown later, these correspond to modulations of the reflected pulse envelope. These may be understood by considering the propagation of a relativistically intense pulse up the density ramp of the target. Because the laser interacts with plasma up to the point when it reflects, effects such as relativistic self-phase modulation (SPM) are able to occur that may significantly modulate the laser spectra [31]. As L_s becomes longer than the electron inertial length, c/ω_p, plasma waves are able to form and couple to the incident wave through parametric instabilities similar to Stimulated Raman Scattering (SRS) or Two-Plasmon Decay (TPD) [32, 33]. In particular, near the quarter critical surface, $n = \frac{1}{4}n_c$, the incident light couples to plasma waves at $\omega_0/2$, which may either modulate the spectrum before the pulse reflects or result in backscattering that can mix with the reflected pulse. As shown analytically [34, 35], TPD and SRS can cause the formation of half-integer harmonics and splitting. For longer L_s, SPM is able to further modulate the spectra and the side-bands devolve into a complicated spectral structure.

Two dimensional numerical simulations were carried out with the particle-in-cell code OSIRIS 2.0 [38]. Simulations were run using a 45.5×45.5 μm^2 square box with 16 particles-per-cell, using a grid of size $10,500 \times 10,500$. This results in a spatial resolution in each dimension of $\lambda/185$, enabling higher-order harmonic frequencies to be resolved in the simulation. The plasma was a slab with density $100n_c$ and a thickness of 551 nm. A variable scale length exponential density was introduced to the front surface of the target representing the pre-plasma, and the target normal was at a 45° angle to the laser propagation direction. L_s was varied over the range $\lambda/100 \leq L_s \leq \lambda$ to determine the impact of the pre-plasma scale length on the harmonic generation. The simulated laser pulse had a normalized vector potential $a_0 = 30$ with a full-width at half-maximum duration of 34 fs. The pulse was focused into a 1 μm diameter Gaussian focal spot on the front surface of the target. The target was located within the box such that the reflected pulse was able to propagate away from the target into a region of vacuum; at this point the fields surrounding the target were masked out, and the reflected light was analyzed using both one and two dimensional fast Fourier transforms.

The two dimensional simulations performed at 45° incidence angle replicate the features of the experimental results, as shown in Fig. 3 (a). The experimental detector solid angle only covers 1.7×10^{-5} sr, so without a measurement of the divergence of the particular harmonic, a total conversion efficiency cannot be easily made. In the simulations, however, such a measurement is trivial. The total conversion efficiency as a function of scale length was found to be a maximum at a point close to c/ω_0. In the simulations, plasma wave formation is observed to occur only when the L_s surpasses c/ω_0. This can be understood by the fact that the largest plasma wavenumber that can be supported is $k_p = c/\omega_p$, which near the critical surface will be c/ω_0.

The conversion efficiency into HOHG was found to increase as L_s increases (Fig. 4 (b)), which is simply be-

cause of the decreased restoring force due to charge separation that results in an increased oscillation amplitude for the moving plasma mirror. However, once L_s was large enough, $L_s \gtrsim c/\omega_0$, the energy in the harmonics was reduced because of transfer of energy in generating plasma waves. In addition, the time and space dependent modulations introduced by the surface plasma waves lead to a loss of coherence. Although Fig. 4 shows the conversion efficiency along the specular direction, the total conversion efficiency is peaked at the same L_s as in the specular case. To isolate and establish the effects of the instabilities, 1D PIC simulations were also performed with circular polarization at normal incidence. The circular polarization suppresses absorption effects and harmonic generation, so that the dominant physical effects are limited to the plasma wave generating instabilities. Varying L_s at a given intensity, the reflected spectra can be compared with that of the incident spectra, providing a measure of how much of the fundamental frequency has been converted to sidebands. In Fig. 4 (a) it can be seen that the change remains small until a point where the spectra exponentially increases, occurring near c/ω_0. The absorption in the simulation is shown in Fig. 4 (b); and is also observed to display a similar increase above the nominal L_s as energy is absorbed from the laser pulse to produce a plasma wave, reducing the efficiency.

The presence of periodic features in the spectrum, such as half-harmonics, may be understood with the following heuristic model. Using a slowly varying envelope approximation, an attosecond pulse train may be described by a summation of identically shaped individual pulses with amplitude and phase variations [21]. Let the shape of a pulse be given by $f(\xi - \xi_n)$, where $\xi = \frac{x}{c} - t$ is the phase coordinate and the pulse envelope $E_0(\xi)$ provides the amplitude of each individual pulse. When the electrons at the reflecting surface experience a "gamma spike" [36], or a rapid increase in the Lorentz factor $\gamma = \frac{1}{\sqrt{1-(v/c)^2}}$, high harmonics are generated with the times of generation (phase compression) represented by ξ_n. The reflected field can therefore be described by $E_R = E_0(\xi)\sum_n f(\xi - \xi_n)$. This may be rewritten as $E_r = E_0(\xi)(f * D(\xi))$, where $*$ denotes the convolution of $f(\xi)$ with a function $D(\xi) = \sum_n \delta(\xi - \xi_n)$. The Fourier spectrum of this radiation, $\tilde{I}_r(\omega) = \tilde{E}_r^2$, may therefore be expressed as $\tilde{I}_r = \left|\tilde{E}_0 * (\tilde{f}\tilde{D})(\omega)\right|^2$.

If the attosecond pulse train is evenly spaced, then $D(\xi)$ is simply a Dirac comb, whose Fourier transform is similarly a frequency comb representing harmonics of the fundamental. The shape factor of an attosecond pulse determines the overall bandwidth of the harmonic frequency comb. Since the frequency comb is convolved with $\tilde{E}_0$, the shape of the laser envelope determines the shape of each harmonic, giving rise to the features found in Fig. 2. For the case that an $\omega/2$ envelope modulation, e.g. parametric instabilities at the quarter critical density surface, half harmonics will appear in the spectrum. Likewise, an envelope modulation of the form $E_0(\xi) \propto 1 + \epsilon\sin(\xi\Delta\omega)$, e.g. from the beating of SRS light with frequency difference $\Delta\omega = \omega_p$ from the fundamental, will lead to identical satellites on the harmonics. If the attosecond pulse train is no longer evenly spaced, e.g. due to a chirp on the drive pulse, or bulk motion of the surface due to radiation pressure, the harmonic structure will be effectively lost.

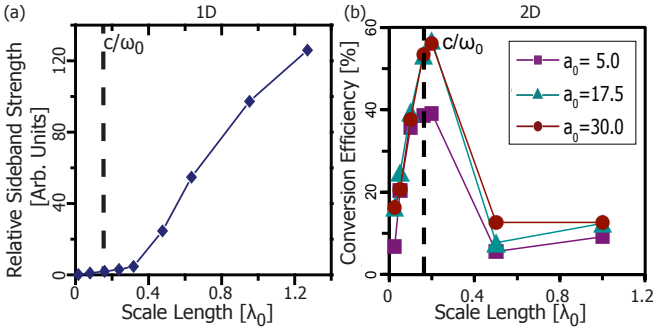

FIG. 4. (Color online) The conversion of fundamental laser frequency into other frequencies as a function of scale length from 1D simulations of a circular polarized pulse are shown in (a). Since harmonic generation is minimized for circular polarization, the rapid rise in conversion of fundamental laser frequency to sidebands due to parametric instabilities can be observed clearly. The conversion efficiency into high harmonic generation from the 2D simulations is shown in (b) for both an a_0 of 5 (squares), 17.5 (triangles), and 30 (circles) along the specular direction. The optimal scale length occurs close to the plasma wavelength of c/ω_0 which occurs near 0.2λ.

Another interesting feature in the simulations is that for intensities varying between an a_0 of 5 to 30 the maximum conversion efficiency occurs for very similar scale lengths even though the laser penetrates to very different densities defined by the relativistic critical density, as shown in Fig. 4 (b), and even the overall conversion efficiency has a very weak dependence on a_0. This suggest a universality in L_s for dramatically different intensities. Some dynamics of a high intensity laser-plasma interaction may be described using the similarity parameter $S = \frac{n_e}{n_c a_0}$ provided $a_0 \gg 1$ [37]. For such high intensities, the relativistic critical density is $n_c^{Rel.} \approx n_c a_0$, or simply the point at which $S = 1$. The function describing the electron density profile becomes $n_e = n_c^{Rel}\exp(-X/\Lambda)$, where X is normalized via $X = S^{\frac{1}{2}}\omega_0 x/c$ and Λ is the (normalized) scale length. Since $S = 1$ at the point of reflection, and the system is expected to be self-similar for fixed S, the dynamics are independent of a_0 for an exponential density profile with (unnormalized) scale length $L_s = \frac{c\Lambda}{\omega_0}$.

In conclusion, an optimal scale length was determined to exist for strongly relativistic intensities. The optimum

is due to a balance between requiring a longer scale length so that the plasma electrons can be effectively displaced allowing efficient movement of the critical density surface and requiring a short enough scale length as not to drive parametric instabilities. Although for longer scale lengths significant radiation is produced, the necessary coherence for attosecond pulse generation was lost (Fig. 3 (b)) . Examining the plasma wave formation for longer scale lengths in 2D simulations, it can be seen that the surface plasma wave are of large amplitudes and therefore strongly modulate the pulse resulting in a loss of coherence in the reflected wave. These two competing requirements lead to an optimum close to c/ω_0. In addition, the special self-similarity of an exponential profile means that this optimum does not depend on intensity. Realistically, an upper limit in intensity invariance should exist, since the exponential density profile is truncated at some maximum density, which breaks the self-similarity. However, even for low atomic number solid density plasmas ($n > 100\ n_c$) this would require a temporally clean pulse with intensity $I \gg 10^{22}$ Wcm^{-2}. Hence, provided the target is not relativistically optically transparent, the only parameter that determines the optimal plasma dynamics for harmonic generation is the pre-plasma scale length, L_s, with optimum efficiency for $L_s = \frac{c}{\omega_0}$.

This work was supported by the National Science Foundation through Grant No. PHY-0114336, Grant No. PHY-0810979, Grant No. PHY-1054164, the Department of Energy through Grant No. ER55145, and the Graduate Research Fellowship Program Grant No. DGE-0718128. We acknowledge the OSIRIS consortium (UCLA/IST Portugal) for the use of the OSIRIS 2.0 framework. Simulations were performed on the Nyx Cluster at Univ. of Michigan.

* Present address:JILA, University of Colorado, Boulder, CO 80309, USA

[1] S. Kneip, *et al.*, Nat. Phys. **6**, 980 (2010).
[2] I. McKinnie, and H. Kapteyn, Nat. Phot. **4**, 149 (2010).
[3] S. V. Bulanov, *et al.*, Phys. Plasm. **1**, 745 (1994).
[4] D. von der Linde and K. Rzàzewski, App. Phys. B **63**, 499 (1996).
[5] R. Lichters, *et al.*, Phys. Plasm. **3**, 3425 (1996).
[6] P. A. Norreys, *et al.*, Phys. Rev. Lett. **76**, 1832 - 1835 (1996).
[7] L. Plaja, L. Roso, K. Rzàzewski, and M. Lewenstein, J. Opt. Soc. Am. **7**, 1904 (1998).
[8] N. M. Naumova, J. A. Nees, I. V. Sokolov, B. Hou, G. A. Mourou, Phys. Rev. Lett. **92**, 063902 (2004).
[9] U. Teubner, P. Gibbon, Rev. Mod. Phys. **81**, 445-479 (2009).
[10] N. H. Burnett, H. A. Baldis, M. C. Richardson, G. D. Enright, App. Phys. Lett. **31**, 172-174 (1977).
[11] R. L. Carman, D. W. Forslund, J. M. Kindel, Phys. Rev. Lett. **46**, 29-32 (1981).
[12] B. Dromey, *et al.*, Nat. Phys. **2**, 456 - 459 (2006).
[13] V. Yanovsky, *et al.*, Opt. Exp., **16**, 2109 (2008).
[14] B. Dromey, *et al.*, Nat. Phys. **8**, 804-808 (2012).
[15] S. Gordienko, *et al.*, Phys. Rev. Lett. **93**, 115002 (2004).
[16] T. Baeva, *et al.*, Phys. Rev. E **74**, 046404 (2006).
[17] P. Mora, Phys. Rev. Lett. **90**, 185002 (2003).
[18] R. Fedosejevs, *et al.*, Phys. Rev. Lett. **64**, 1250 (1990).
[19] M. I. Santala, *et al.*, Phys. Rev. Lett. **84**, 1459 (2000).
[20] A. G. Mordovanakis, *et al.*, Phys. Rev. Lett. **103**, 235001 (2009).
[21] M. Behmke, *et al.*, Phys.Rev. Lett. **106**, 185002 (2011).
[22] C. Rödel, *et al.*, Phys. Rev. Lett. **109**, 125002 (2012).
[23] R. Lichters, J. Meyer-ter-Vehn, Inst. Phys. Conf. Ser. **154**, 221-230 (1996).
[24] V. Chvykov, P. Rousseau, S. Reed, G. Kalinchenko, V. Yanovsky, Opt. Lett. **31**, 1456 (2006).
[25] B. Dromey, S. Kar, M. Zepf, P. Foster, Rev. Sci. Inst. **75**, 645 (2004).
[26] G. Doumy, F. Quéré, O. Gobert, M. Perdrix, P. Martin, P. Audebert, J. C. Gauthier, J. P. Geindre, T. Wittmann, Phys. Rev. E **69**, 026402 (2004).
[27] F. Dollar, *et al.*, Phys. Rev. Lett. **108** 175005 (2012).
[28] J. T. Larson, S. M. Lane, Journ. Quant. Spect.Rad. Trans. **51**, 179 (1994).
[29] M. Zepf, *et al.*, Phys. Rev. E **58**, 5253 (1998).
[30] J. H. Easter, *et al.*, Opt. Lett. **35**, 3186 (2010).
[31] I. Watts, *et al.*, Phys. Rev. E **66**, 036409 (2002).
[32] R. W. Wellwarth, Phys. Rev. **130**, 1850 (1963).
[33] C. S. Liu, M. N. Rosenbluth, Phys. Fluids **19**, 967 (1976).
[34] H. C. Barr, *et al.*, Phys. Rev. Lett. **83**, 1606 (1999).
[35] H. C. Barr, *et al.*, Phys. Plasm. **7**, 2604 (2000).
[36] T. Baeva, *et al.*, Phys. Rev. E **74**, 046404 (2006).
[37] S. Gordienko, A. Pukhov, Phys. Plasm. **12**, 043109 (2005).
[38] R. O. Fonseca, *et al.*, Lect. Notes Comput. Sci. **2331**, 342 (2002).